# Selective Excited State Dynamics in a Unique Set of Rationally Designed Ni Porphyrins

Brian Pattengale,<sup>†</sup> Qiuhua Liu,<sup>‡</sup> Wenhui Hu, <sup>†</sup> Sizhuo Yang, <sup>†</sup> Peilei He, <sup>†</sup> Sir Lawrence Tender, <sup>†</sup> Yingqi Wang,<sup>§</sup> Xiaoyi Zhang, <sup>‡</sup> Zaichun Zhou,<sup>‡\*</sup> Jian Zhang, <sup>\*</sup>, and Jier Huang<sup>†\*</sup>

†Department of Chemistry, Marquette University, Milwaukee, WI 53201, USA

‡Key Laboratory of Theoretical Organic Chemistry and Functional Molecules, Ministry of Education; and School of Chemistry and Chemical Engineering, Hunan University of Science and Technology, Xiangtan 411201, China

§Center for High Pressure Science and Technology Advanced Research, Shanghai 201203, China LX-ray Science Division, Argonne National Laboratory, Argonne, Illinois, 60349, USA Molecular Foundry, Lawrence Berkeley National laboratory, Berkeley, California 94720, USA

## **Corresponding Author**

\*Jier Huang (jier.huang@marquette.edu)

\*Jian Zhang (jzhang3@unl.edu)

\*Zaichun Zhou (<u>zhouzaichun@hnust.edu.cn</u>)

ABSTRACT. In this work, we report the design and photophysical properties of a unique class of Ni porphyrins, in which the tert-butyl benzene substituents at the -meso positions of the macrocycle were tethered by ethers with alkyl linkers. This not only results in the permanently locked *ruf* distortion of the macrocycle but also enables the engineering of the degree of distortion through varying the length of alkyl linkers, which addressed the complication of uncertainty in the specific structural distortions that has long plagued the porphyrin photophysical community. Using advanced time-resolved optical and X-ray absorption spectroscopy, we observed tunable excited state relaxation pathway with the degree of distortion as well as the transient intermediate structure associated with that, providing a new avenue to afford the accessibility to a wide range of excited state properties in nonplanar porphyrins.

### Introduction.

Metalloporphyrins represent versatile model systems for various biophysical processes ranging from photosynthesis, oxygen transport, and oxygen activation.<sup>1-3</sup> The active research on these systems in the past decades has significantly advanced the understanding of their structure and photochemical properties, which in turn led to the discovery of many new applications including photodynamic therapy, <sup>4,5</sup> light emitting diodes, <sup>6,7</sup> and solar energy conversion. <sup>8-10</sup> Previous studies on their electronic and photophysical properties demonstrated that the macrocycle ring in metalloporphyrins is highly flexible and often undergoes various deformations from planarity due to functionalization with bulky peripheral substituents, which dramatically alters their chemical and photophysical properties from their planar analogues. 11,12 For example, nonplanar distortion due to either ruf or sad deformation can tune the redox potential, 13-15 axial binding affinity of center metal, 14,16,17 and basicity of N atoms etc., 18,19 the properties that directly dictate their biological function for proteins with porphyrin cofactor. Substituent-induced non-planar distortion can also significantly impact the ground state optical properties and energetic ordering of excited states, leading to tunable relaxation dynamics, 12,18,20-30 which are the key photophysical properties that determine the light harvesting and charge transport function of photosynthetic pigments in proteins and solar energy conversion.

While these previous studies have certainly provided important insight on the correlation of electronic and chemical properties of metalloporphyrins with macrocycle conformational distortion, the distortion was achieved via substitution of the -meso or -β positions of the porphyrin periphery with steric crowding substituents. <sup>11,31,32</sup> Under these conditions, different conformations can be adopted by the macrocycle and perturbed by external environment, leaving significant uncertainty in probing their structural features and photophysical properties. Moreover, the

**Scheme 1.** Design principle of permanently distorted Ni porphyrins.

assignment of *sad*, *ruf*, or other distortions largely rely on calculations or crystal structures, which are certainly dynamic in the solution phase where photophysical studies are performed. As a result, it is highly needed to have a permanently locked model system for which the distortion is known to be one of the fixed distortions such that the effects of the specific distortion on the chemistry and photochemical behavior can be unambiguously determined and distinguished from the effects of other types of distortions. In this work, we report the design and photophysical studies of a unique class of Ni porphyrins (Scheme 1), in which the *-meso* positions of the macrocycle were tethered by ethers that are attached to the t-butyl benzene substitutes.<sup>33</sup> Using advanced time-resolved optical and X-ray absorption spectroscopy, we observed tunable excited state relaxation pathway with the degree of distortion as well as the transient intermediate structure associated with that.

## Experimental.

**Synthesis.** Strapped nickel porphyrin L8-Ni was prepared according to previously published standard methods.<sup>33</sup> 2,2'-[Octane-1,8-diylbis(oxy)]di(5-tert-butyl)benzaldehyde (4.66 g, 10 mmol), and bis(2-pyrrolyl)-4-nitrophenyl-methane (5.34 g, 20 mmol) were added to a boiling propionic/butyric (2:1, v/v) acid mixture (200 mL) in small portions within 5 min. Ni(OAc)<sub>2</sub>·4H<sub>2</sub>O (~2.7 g, 11 mmol) was added to the solution after 15 min under reflux; the mixture was further stirred for 45 min, and then the mixed acids were removed under reduced pressure. The solid

residue was extracted three times with dichloromethane. The extracting solution was washed five times with water and dried with sodium sulfate. After removal of the solvent, the residue was separated by silica gel column chromatography with dichloromethane/petroleum ether (1:2, v/v) to give the purple solid L8-Ni 1.27 g. yield 12.5%. UV-vis (chloroform, 293 K):  $\lambda$ max = 421, 510, 578 nm. HR MS (ESI): found for C<sub>60</sub>H<sub>56</sub>N<sub>6</sub>NiO<sub>6</sub> [M]+ 1014.3616; calcd 1014.3609. All reagent-grade reactants and solvents were used as received from chemical suppliers.

Characterization. UV-Visible spectroscopy was performed using an HP Agilent 8453 spectrometer. High solution Mass spectrum was obtained by using a Varian QFT-MALDI mass spectrometer. Crystal structure determination by X-ray diffraction was performed by using a Bruker SMART 1000 CCD diffractometer equipped with a normal focus, 2.4 kW sealed-tube X-ray source, using monochromatic Mo-K $\alpha$  ( $\lambda$  = 0.71073 A) radiation. A suitable single crystal of each compound was glued to a thin glass fiber with superglue. The SMART program package was used to determine the unit-cell parameters and for data collection. The structure was solved by direct methods and were refined on F2 by the full-matrix least-squares method by using the SHELXT-97 program. The positional parameters for the Ni, N, and O atoms were obtained by direct methods for the compound. All hydrogen atoms were placed geometrically and were refined by riding on their appropriate O and C atoms. The final positions of all non-hydrogen atoms were refined anisotropically. Crystals of L8-Ni was obtained by solvent diffusion in chloroform and methanol.

**Optical Transient Absorption (OTA).** OTA measurements were performed using a Spectra Physics Solstice Ti:Sapphire amplifier (120ps fwhm, 800 nm, 1kHz). Pump pulses were generated with a TOPAS OPA using 75% of the Ti:Sapphire output, and were chopped at 500 Hz for transient absorption measurement. A portion of the remaining 800nm output was directed into a Helios

transient absorption spectrometer (Ultrafast Systems). Time delay between the pump and probe is achieved by a delay stage on the probe line (800nm). The probe is then focused onto a sapphire crystal for white light generation (430nm – 780nm). Samples were prepared in a screw-top 2mm quartz cuvette with PTFE-lined septa. The concentration was 0.1 mM in toluene, purged with N<sub>2</sub> before measurement. The sample was stirred during measurement using a magnetic stirrer and PTFE-coated stir bar. UV-Visible spectroscopy was used to confirm that laser exposure did not result in sample decomposition. Soret band or Q-band excitations were performed, respectively, using 420 nm or 530 nm pulses with 0.3μJ/pulse.

Nanosecond transient absorption measurements were performed using an Edinburgh Instruments LP900 flash photolysis spectrometer. The pump pulse was generated by an Nd:YAG (SpectraPhysics, INDI-10) with third harmonic (355nm) output. The 355nm output was converted to 525nm using an optical parametric oscillator (Spectra Physics). The probe source is a pulsed 450 W Xenon arc lamp, which was detected before and after laser exposure by the integrated CCD detector.

X-ray Transient Absorption Spectroscopy (XTA). XTA was performed at the Advanced Photon Source at Argonne National Laboratory in beamline 11-ID-D. The storage ring was under standard operating mode, with 80 ps fwhm X-ray pulses that were used as the probe. The 100 fs 400nm pump pulse (535 mW) was the second harmonic output of an Nd:YLF Ti:Sapphire regenerative amplified laser at 10 kHz. The sample (1 mM in toluene) was placed in an N₂-purged double-walled flask cooled to 5 degrees C and was continuously flowed through a stainless steel tube using a peristaltic pump to produce a 550 μM sample jet. The jet is positioned between two avalanche photodiodes that collect the X-ray fluorescence signals. Soller slits with Co filters were positioned between the sample and photodiode detectors. Delay-scans were collected at the peak

of the negative XTA difference signal, which corresponded to the on-edge 1s-p<sub>z</sub> feature, the largest feature in the difference spectrum. The full-energy range EXAFS spectra were then collected at the pump delay that produced the largest difference signal, approximately 50 ps for all samples. Because the FWHM of X-ray pulses are 80 ps, the difference spectrum observed is insensitive to pump delay, as XTA can only probe the cooled MC state in Ni porphyrins.

X-ray Absorption Data Analysis. XTA produced two X-ray absorption spectra, laser-on and laser-off spectra. The difference signal was generated by laser-on minus laser-off. First, the ground-state (laser-off) spectra were fit using the Artemis module of the Demeter software package. The FEFF models were constructed using a single molecule with atomic coordinates directly taken from the CIF files. In order to accurately quantify the first-shell Ni-N distance, second-shell and multiple-scattering paths were included into the model. The ground-state spectra in XTA experiments were used for steady-state FEFF analysis. The K-range used for the Fourier transform into R-space was approximately 1.7 to 8.6 for all data sets.

Once satisfactory fits were obtained for the ground-state (laser-off) spectra, the laser-on spectra were fit. Because the excitation pulse does not excite all of the molecules in the X-ray beam path, the laser-on spectrum is actually a combination of both excited and non-excited molecules. To account for this, two amplitude-weighted FEFF models were used to fit the data, where the amplitude is the excited state (ES) fraction. The first model was the same model used for the ground-state molecule, with fixed  $\Delta_{enot}$ , N, R, and  $\sigma^2$ . The second model consisted of the same paths, however R and  $\sigma^2$  were allowed to vary to account for their new values in excited molecules. The ES fraction was fixed during this fitting. Various ES fractions were used to determine a reasonable value (Figure S6) by following the R-factor of the resulting fit. It was determined that an ES fraction of 0.3 best represented the set of porphyrins investigated, and was used to determine

ES parameters. Finally, the modeled ES R-space spectrum was generated by a single FEFF model with ES values for R and  $\sigma^2$  with 100% amplitude weighting.

#### Results and Discussion.

As shown in Scheme 1 and Figure S1, the alkyl linker tends to pull two side rings that connected with the *tert*-butyl benzene group, resulting in a locked *ruf* distortion of the macrocycle. Moreover, the degree of distortion can be systematically tuned by varying the length of the ether-tethered alkyl strap group enabling an unambiguous study on the correlation of their conformational distortion with photophysical properties. As shown in Scheme 1, the length of the alkyl group was varied to include 4 C atoms (L4), 6 C atoms (L6), and 8 C atoms (L8). The synthetic details and characterization of permanently distorted Ni porphyrins (L4 and L6) have been reported previously.<sup>33</sup> L8 was prepared in this work to further decrease the degree of distortion, and its synthesis is outlined in experimental section. The ruffling effect should be more pronounced as the chain length reduces from L8 to L4. The crystal structures confirmed this trend (Figure S1 and Table S1), namely, the macrocyclic distortion effectively induces a contraction of N4 core, where the core diameter (*L*<sub>NN</sub>) decreases from 3.89 Å in L8, to 3.81 Å in L6, and 3.78 Å in L4. Such result is related to the compression of size (*L*<sub>CC</sub>) between the tethered *meso* carbon atoms from 6.72 Å, to 6.50 Å, and 6.34 Å, respectively.

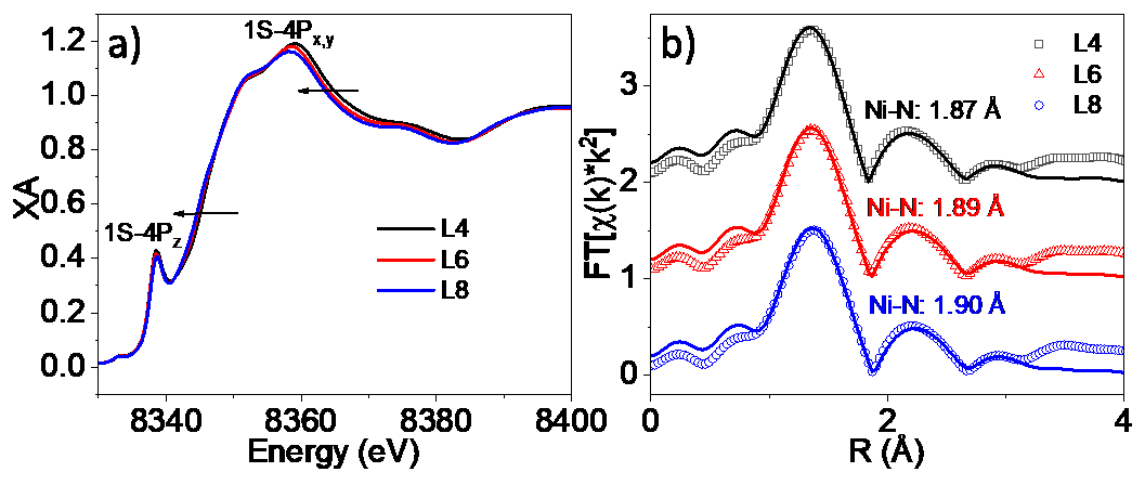


**Figure 1.** (a) XANES spectra for L4-L8 at the Ni K edge. (b) FEFF fitting results of the EXAFS data with the obtained first shell bond distances with uncertainty of approximately  $\pm$  0.02 Å. Data is shown as open points and best fits as solid lines.

The electronic and local structure of the Ni porphyrin analogues were investigated by X-ray absorption spectroscopy (XAS) via the Ni K edge. The X-ray absorption near edge structure (XANES) of each sample are compared in Figure 1a. Two distinct features are observed on the rising edge, including a sharp feature at ~8.338 keV corresponding to the 1S-4Pz transition and the white line transition at the absorption edge (~8.360 keV) corresponding to the 1S-4Px,y transition. 12,25,34 The whole energy spectra show blue-shifts above-edge, suggesting the decrease of the Ni-N bond length from L8 to L4. To gain quantitative insight on the nature of these features, the extended X-ray absorption fine structure (EXAFS) spectra (Figure S2) of these samples were analyzed using FEFF fitting with the Demeter software package. Figure 1b shows the Fourier-transformed R-space spectra along with their best fits. It can be clearly seen that significant decreases of Ni -N first shell bond lengths are observed with decreasing tether length/increasing

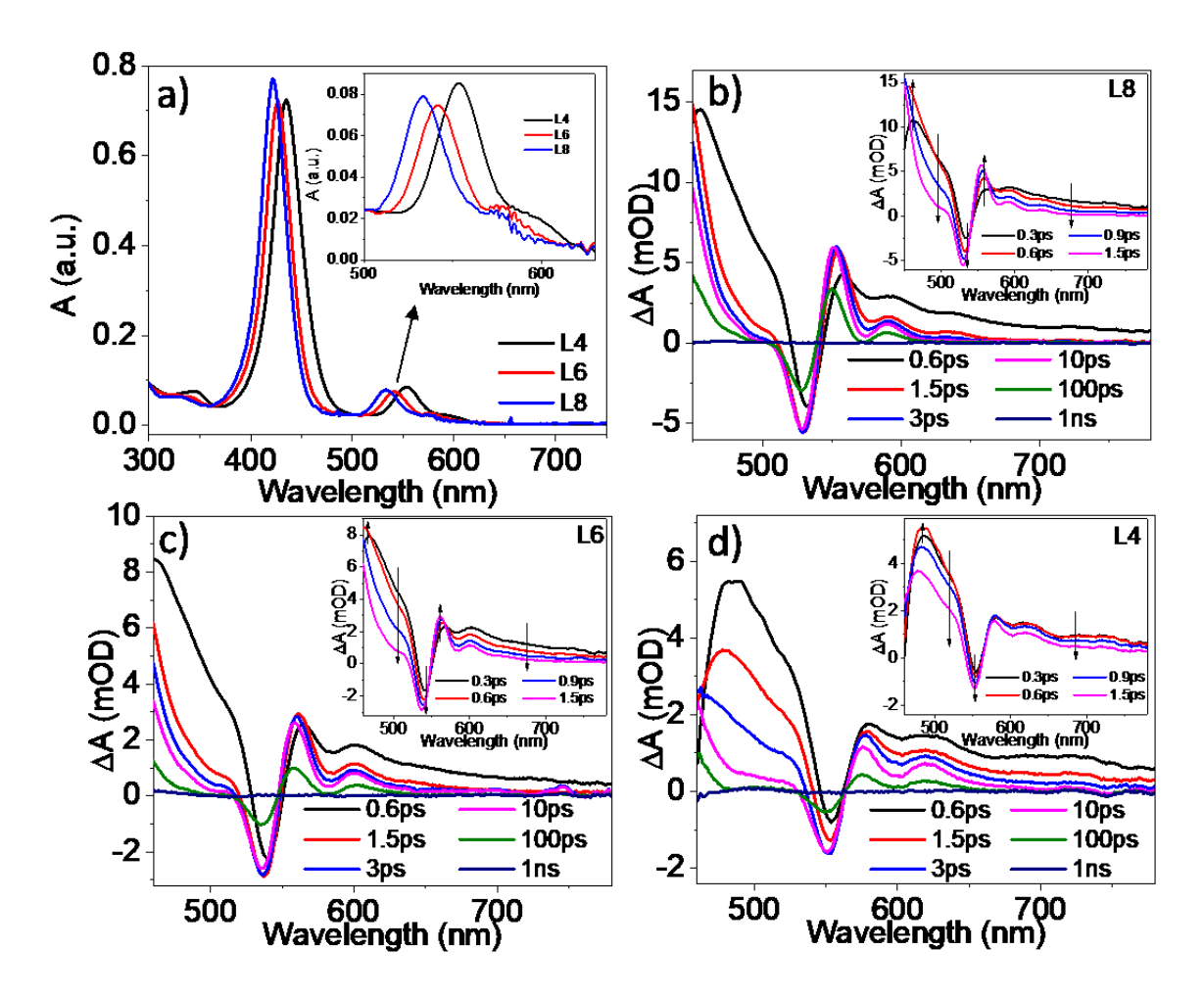


**Figure 2.** UV-visible spectra (a) for Ni-porphyrin analogues with inset showing the expanded Q-band region. OTA spectra after 400 nm excitation of the S<sub>0</sub>-S<sub>2</sub> transition for L8 (b), L6 (c), and L4 (d). Insets of b-d display the early time spectra and highlighted spectral evolution on this timescale.

degree of distortion, indicating that distortion results in closer Ni-N distance, consistent with XANES results. These values are slightly shorter than the average distances observed in the X-ray crystal structure (L8, 1.944 Å; L6, 1.910 Å; L4, 1.892 Å), which is likely explained by the measurement environment and conditions, as XAS was performed in solution phase while the X-ray crystal structures were obtained in solid state. The full FEFF fitting parameters are given in Tables S2-4.

Figure 2a shows the UV-Visible absorption spectra of Ni porphyrins, which are featured by an intense band in the UV region (Soret band,  $S_0$ - $S_2$  transition) and relatively weaker bands in the visible region of the spectrum (Q-band,  $S_0$ - $S_1$  transitions).  $^{11,21,36}$  A clear red-shift trend is observed from L8-L4 as a function of distortion of the porphyrin macrocycle. From the molecular orbital diagrams,  $^{36}$  the lowest energy allowed transitions consist of occupied  $a_{1u}(\pi)$  and  $a_{2u}(\pi)$  initial states and unoccupied  $e_g(\pi^*)$  final states. Upon ruffling of the porphyrin macrocycle, red-shifts in the UV-visible spectra were observed due to destabilization of the  $a_{1u}(\pi)$  and  $a_{2u}(\pi)$  molecular orbitals.  $^{11,20}$  Therefore, the trend observed in L8-L4 demonstrates that systematic distortion results in shifting of the Soret band (Figure 2a) and Q-band (inset) transition energies, consistent with literature reports.

Femtosecond optical transient absorption spectroscopy (OTA) was performed to investigate the excited state dynamics of these Ni porphyrins. Figure 2b-d show the OTA spectra for L8, L6, and L4, respectively, following 400 nm excitation which triggers Soret band transition. The initial spectrum of the least-distorted sample L8 (0.3 ps, inset of Figure 2b) is featured by a positive band in the 460-500 nm region, broad absorption at 550-780 nm region, and a bleach band centered at ~530 nm that can be assigned to the ground state bleach (GSB) of Q-band. Distinct spectral evolutions were observed for these features within 2 ps, including the decay of the positive feature at 460-500 nm, the growth of the Q-band GSB, decay of the 550-780 nm absorption, and the formation of a positive feature at 553 nm. The presence of a clear isosbestic point at 562 nm between the latter two features suggest these evolutions correspond to same relaxation process. Because similar spectral evolution was observed in the TA spectra following Q-band excitation (Figures S3), this evolution cannot be attributed to the relaxation of S2-S1. In addition, the absence of stimulated emission following the Soret band excitation excludes the contribution from the S1

state. These results, which are in good agreement with previous reports that  $S_2$ - $S_1$  and  $S_1$ -  $(3d_{x^2-y^2}, 3d_{z^2})$  (denoted as (d,d)) relaxation is ultrafast and beyond our instrument resolution of 300 fs, suggest that the early time spectral evolution can be attributed to intramolecular vibrational relaxation (IVR) from the hot (d,d) state.  $^{22-24,27,37-39}$  After that, the OTA spectra show two more distinct spectral evolutions, including 1) the whole spectrum shows slight blue-shift which is accompanied by relatively slow decay within 2-20ps, and 2) the simultaneous decay of all transient features without spectral shift > 20 ps. While the spectral evolution for the latter can be attributed to the returning of transient species to the GS, we assign the former to the vibrational cooling (VC) process from a hot (d,d) state to cooled (d, d) configuration.  $^{34-36}$  While L6 (Figure 2c) appears to show similar dynamics to L8, significantly slower spectral changes on both the VC and IVR timescales in the more distorted L4 analogue (Figure 2d), as well as shorter ES lifetime.

To quantitatively understand these relaxation dynamics and elucidate trends as a function of structural distortion, we fit the decay kinetics at the described spectral regions with multiexponential rise/decay functions. The excited state absorption (ESA) in Figure 3a is described predominantly by slow processes relative to the ESA in Figure 3b. From the Q-band bleach (Figure 3c), it is evident that the early-time growth on a linear scale is followed by at least 2 distinct decay components as revealed by log-scaling after the break. Based on both the kinetic and spectral observations, a triexponential model was employed to quantitatively describe the excited state dynamics, with fitting parameters shown in Table 1. For nearly all traces,  $\tau_1$ , corresponding to an intramolecular vibrational redistribution (IVR) process , is 0.5 ps for L6, L8 and 1.33 ps for L4, although for L6 and L8,  $\tau_1$  corresponds to a rise in the 562 nm and 553 nm traces, respectively. The Q-band bleach also rises for all samples with  $\tau_1$ , in agreement with the spectral observations. After IVR, the kinetics for L4 are markedly different from that of L6 and L8 with a trend at some

wavelengths, most clearly demonstrated in the positive feature on the red-side of the Q-band bleach (Figure 3d). At this feature, τ<sub>2</sub> which represents vibrational cooling (VC) is fit with a growth component in L8 while L6 and L4 decay in this region. This process is accompanied by a growth in the Q-band bleach in L4, while L6 and L8 show Q-band decay for τ<sub>2</sub>. Finally, τ<sub>3</sub>, which corresponds to the return of cooled (d,d) state to GS, shows a clear trend with respect to structural distortion, where L8 has the longest lifetime and L4 has the shortest. The ESA at 690 nm (Figure

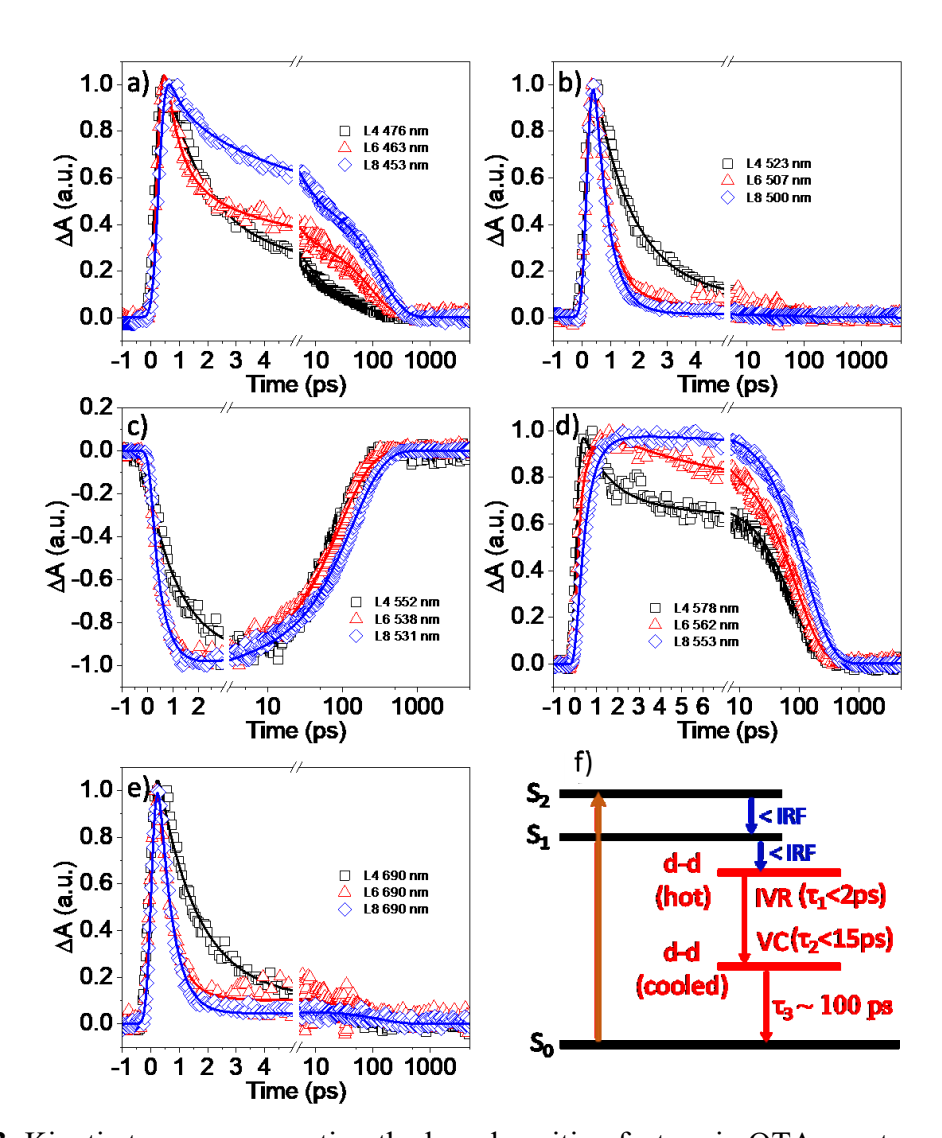
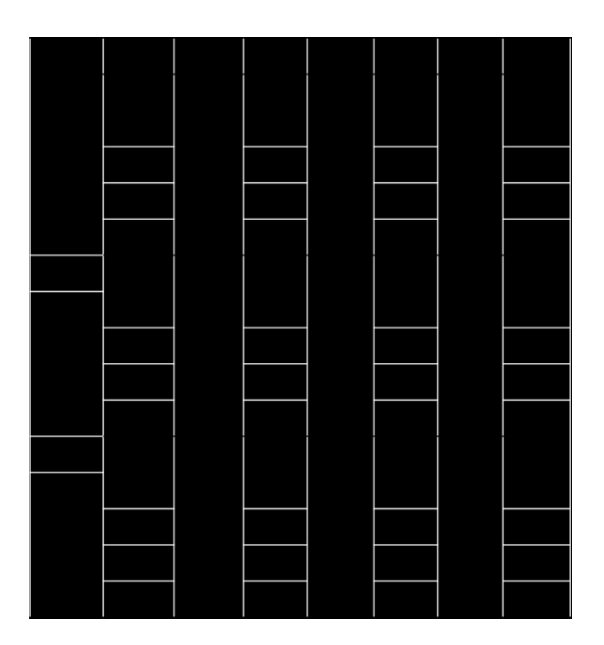


**Figure 3.** Kinetic traces representing the broad positive feature in OTA spectra on the blueside of Q-band bleach (a,b), Q-band bleach (c), derivative-shaped positive feature (d), and broad vis-NIR feature probed at 690 nm (e). (f) Scheme showing the three-component model used to fit OTA data.

3e) closely resembles the decay at the probe wavelengths shown in Figure 3b. A scheme showing the fit model is presented in Figure 3f. The Q-band excitation data could be fit by the same model (Figure S4, Table S5), implying that the same relaxation processes are observed regardless of excitation wavelength.

**Table 1.** OTA kinetic fit parameters, Soret excitation.



The differences observed at OTA imply a fundamental difference in the excited state relaxation cascades as a function of structural distortion. For L4, both  $\tau_1$  and  $\tau_2$  are longer but  $\tau_3$  is shorter than those in L8 and L6, which directly implies that the more distorted (d, d) state could prevent the IVR and IC relaxation while facilitate the relaxation from cooled (d, d) state to GS. This dependence of the excited state deactivation pathway on the degree of distortion is unprecedented for Ni porphyrins. One explanation for the slower IVR and VC processes is related to the relaxation to the cooled d-d state being radiationless and depositing ca. 10,000 cm<sup>-1</sup> of energy into macrocycle vibrational modes. However, the highly distorted L4 porphyrin is most restricted to *ruf* modes and, therefore, has less vibrational degrees of freedom than L6 and L8.

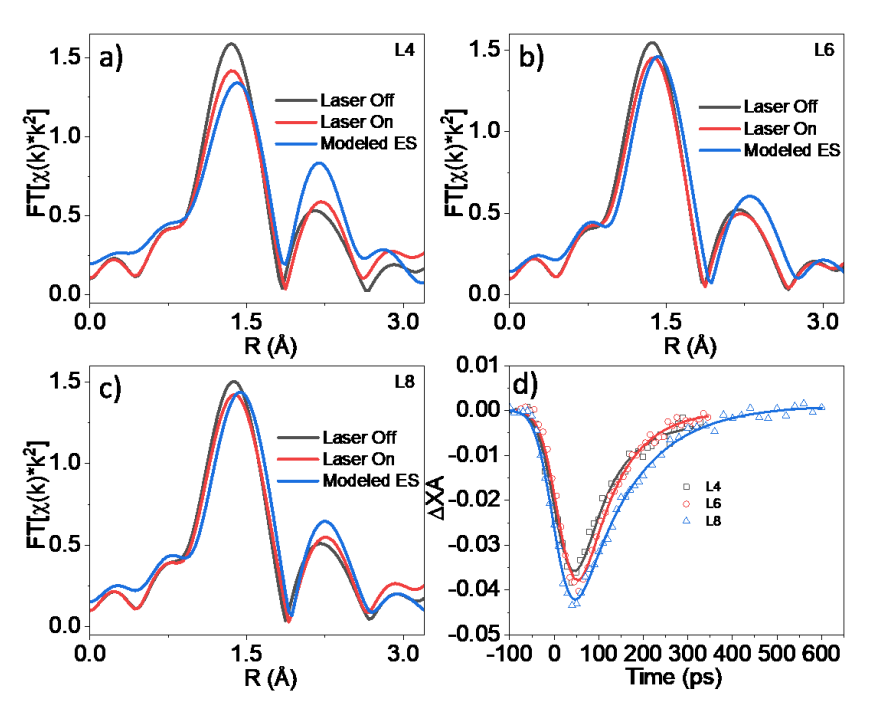


**Figure 4.** R-space data for XTA experiments. Laser off, laser on, and modeled ES spectra in R-space for L4 (a), L6 (b), and L8 (c). The ES Ni-N distance is shown in each figure. Delay scans at the maximum negative difference signal for L4-L8 and best fits (d).

The highly-altered photodynamics for the most highly-distorted L4 porphyrin might suggest that the final Ni d-d state ( $3d_{x^2-y^2}$ ,  $3d_{z^2}$ ) that forms via vibrational relaxation through the macrocycle modes<sup>26,40</sup> could be different in nature for L4 compared to L6 and L8. To investigate the nature of the vibrationally cooled state, X-ray transient absorption was performed at the Ni K-edge, which has previously been used to demonstrate the Ni d-d ( $3d_{x^2-y^2}$ ,  $3d_{z^2}$ ) character of the final state.<sup>24</sup> In the current study, the FWHM of synchrotron pulses used for time-resolved measurements is approximately 80 ps, which can only probe the MC state. XTA experiments were performed using 400nm laser pump and Ni K-edge X-ray probe (Figure S5). The laser-off spectra constitute the GS spectra while the laser-on spectra represent a combination of ES molecules excited by the laser pulse and GS molecules that were not excited. Therefore, an ES fraction was incorporated into the FEFF fitting model in order to extract ES information (Figure S6).

FEFF fitting was performed using the optimized ES fraction of 0.3, meaning that the laser excitation pulse excites 30% of molecules in the X-ray beam path while 70% of molecules remain in their ground state (Figure S7). The resulting fits are shown in Figure 4a-c along with the modeled ES spectrum. From comparison of the peak positions in the first shell representing Ni-N distance, it is qualitatively observable that macrocycle core-expansion about Ni metal center is observed in the ES, in agreement with previous reports.  $^{23,24,27,28,40}$  The fit values for R<sub>ES</sub> indicate that first shell expansion is similar for these samples with expansion occurring from  $1.87 \rightarrow 1.94$  Å for L4 (Figure 4a), from  $1.89 \rightarrow 1.95$  Å for L6 (Figure 4b), and from  $1.90 \rightarrow 1.96$  Å for L8 (Figure 4c). The lifetime of this Ni d-d ( $3d_{x^2-y^2}$ ,  $3d_{z^2}$ ) ES tracked by delay scans (Figure 4d, fit parameters in Table S6) for each sample shows a good agreement with the long-lived state in OTA measurements ( $\tau_3$ ), further supporting that this is the cooled (d, d) state and also confirming that the Ni centered d-d state deactivation is faster in the most distorted analogue.

One of the most interesting findings of this work is that increased distortion leads to faster deactivation of the Ni d-d  $(3d_{x^2-y^2}, 3d_{z^2})$  excited state. The cooled Ni d-d state involving the expanded-core macrocycle involves an interplay between macrocycle and metal-centered states. It has been previously shown that ruffling influences the Ni d-d energetics.<sup>27</sup> Specifically, it was shown for a sterically distorted porphyrin species that the  $3d_{x^2-y^2}$  orbital mixed with the porphyrin  $\pi$  orbitals and resulted in a small degree of charge transfer (CT) from macrocycle to metal. The observation that a larger degree of permanent distortion leads to faster ES decay in this study implies the involvement of the *ruf* mode of the macrocycle in relaxation of the Ni d-d ES. These effects could be a combination of dynamic, including non-adiabatic effects, or static effects.

Interestingly, distortion leads to faster ES deactivation also for free-base analogues in the triplet manifold (Figure S8,9). It can also be observed that the ES features in free-base ns-OTA and Ni-metallated fs-OTA data are significantly broadened as a function of distortion (Figure S10) despite the most distorted macrocycle being the most restricted and having the fewest vibrational degrees of freedom. Therefore, the contribution of dynamic interconversion with out-of-plane modes other than *ruf* can be disregarded. We suggest that anharmonic coupling of various in-plane modes and the *ruf* mode is enhanced due to distortion, leading to broadening of the ES features in both the Ni metallated and free-base cases, and to enhanced ES decay.

#### Conclusion.

In summary, we report the design and photophysical properties of a unique class of Ni porphyrins permanently locked in *ruf* distortion resulting from the tethered *meso* positions of the macrocycle by ethers that are attached to the *tert*-butyl benzene substitutes. We show that by varying the length of ether chains, the degree of distortion can be systematically controlled. Using the combination of advanced OTA and XTA spectroscopy, which allows us to directly probe the structural dynamics of Ni porphyrins, we demonstrate that ES relaxation dynamics can be highly tuned by the degree of distortion. The IVR and VC processes are slowed significantly in permanently distorted porphyrins due to reduced vibrational degrees of freedom. Furthermore, it was shown that the lifetime of the final Ni d-d state formed in the relaxation cascade is dependent on the degree of distortion, where higher distortion leads to enhanced ES decay. These results suggest that these permanently-distorted porphyrins are a useful scaffold for investigating macrocycle-metal ES dynamics, implying vast utility in the porphyrin community.

#### ASSOCIATED CONTENT

Supplementary Information including experimental, supplementary ns-OTA results, XAS figures, Q-band excitation OTA results are available free of charge.

#### **AUTHOR INFORMATION**

#### Notes

The authors declare no competing financial interests.

#### ACKNOWLEDGMENT

This work was supported by National Science Foundation (CBET-1706971) and ACS-PRF (57503-DNI6). Use of the Advanced Photon Source at Argonne National Laboratory was supported by the U. S. Department of Energy, Office of Science, Office of Basic Energy Sciences, under Award No. DE-AC02-06CH11357. Brian Pattengale acknowledges the John J. Eisch fellowship during the 2017-2018 academic year. We thank the Energy Sciences Institute at Yale University for use of the ns-OTA flash photolysis spectrometer.

#### REFERENCES

- (1) Gust, D.; Moore, T. A.; Moore, A. L. Mimicking Photosynthetic Solar Energy Ttransduction. *Acc. Chem. Res.* **2001**, *34*, 40-48.
- (2) Holten, D.; Bocian, D. F.; Lindsey, J. S. Probing Electronic Communication in Covalently Linked Multiporphyrin Arrays. A guide to the rational design of molecular photonic devices. *Acc. Chem. Res.* **2002**, *35*, 57-69.
- (3) Rodriguez, J.; Kirmaier, C.; Holten, D. Optical-Properties of Metalloporphyrin Excited-States. *J. Am. Chem. Soc.* **1989**, *111*, 6500-6506.
- (4) Khalid, L.; Mroz, P. Imidazole Metalloporphyrins as Photosensitizers for Photodynamic Therapy: Role of Molecular Charge, Central Metal and Hydroxyl Radical Production. *Eur. J. Med. Chem* **2009**, *14*, 4-4.
- (5) Mroz, P.; Bhaumik, J.; Dogutan, D. K.; Aly, Z.; Kamal, Z.; Khalid, L.; Kee, H. L.; Bocian, D. F.; Holten, D.; Lindsey, J. S. et al. Imidazole Metalloporphyrins as Photosensitizers for Photodynamic Therapy: Role of Molecular Charge, Central Metal and Hydroxyl Radical Production. *Cancer Lett.* 2009, 282, 63-76.

- (6) Graham, K. R.; Yang, Y. X.; Sommer, J. R.; Shelton, A. H.; Schanze, K. S.; Xue, J. G.; Reynolds, J. R. Extended Conjugation Platinum(II) Porphyrins for Use in Near-Infrared Emitting Organic Light Emitting Diodes. *Chem. Mater.* **2011**, *23*, 5305-5312.
- (7) O'Brien, D. F.; Baldo, M. A.; Thompson, M. E.; Forrest, S. R. Improved Energy Transfer in Electrophosphorescent Devices. *Appl. Phys. Lett.* **1999**, *74*, 442-444.
- (8) Hasselman, G. M.; Watson, D. F.; Stromberg, J. R.; Bocian, D. F.; Holten, D.; Lindsey, J. S.; Meyer, G. J. Theoretical Solar-to-Electrical Energy-Conversion Efficiencies of Perylene-Porphyrin Light-Harvesting Arrays. J. Phys. Chem. B 2006, 110, 25430-25440.
- (9) Dabestani, R.; Bard, A. J.; Campion, A.; Fox, M. A.; Mallouk, T. E.; Webber, S. E.; White, J. M. Sensitization of Titanium-Dioxide and Strontium-Titanate Electrodes by Ruthenium(Ii) Tris(2,2'-Bipyridine-4,4'-Dicarboxylic Acid) and Zinc Tetrakis(4-Carboxyphenyl)Porphyrin an Evaluation of Sensitization Efficiency for Component Photoelectrodes in a Multipanel Device. *J. Phys. Chem.* **1988**, *92*, 1872-1878.
- (10) Campbell, W. M.; Burrell, A. K.; Officer, D. L.; Jolley, K. W. Porphyrins as Light Harvesters in the Dye-Sensitised TiO<sub>2</sub> Solar Cell. *Coord. Chem. Rev.* **2004**, *248*, 1363-1379.
- (11) Haddad, R. E.; Gazeau, S.; Pécaut, J.; Marchon, J.-C.; Medforth, C. J.; Shelnutt, J. A. Origin of the Red Shifts in the Optical Absorption Bands of Nonplanar Tetraalkylporphyrins. *J. Am. Chem. Soc.* **2003**, *125*, 1253-1268.
- (12) Barkigia, K. M.; Renner, M. W.; Furenlid, L. R.; Medforth, C. J.; Smith, K. M.; Fajer, J. Crystallographic and EXAFS Studies of Conformationally Designed Nonplanar Nickel(II) Porphyrins. *J. Am. Chem. Soc.* **1993**, *115*, 3627-3635.
- (13) Waditschatka, R.; Kratky, C.; Jaun, B.; Heinzer, J.; Eschenmoser, A. Chemistry of Pyrrocorphins Structure of Nickel(Ii) Ccccc-Octaethyl-Pyrrocorphinate in the Solid-State and in Solution Observation of the Inversion Barrier between Enantiomorphically Ruffled Conformers. *Chem. Commun.* **1985**, *22*, 1604-1607.
- (14) Barkigia, K. M.; Chantranupong, L.; Smith, K. M.; Fajer, J. Structural and Theoretical-Models of Photosynthetic Chromophores Implications for Redox, Light-Absorption Properties and Vectorial Electron Flow. *J. Am. Chem. Soc.* **1988**, *110*, 7566-7567.
- (15) Kadish, K. M.; Vancaemelbecke, E.; Boulas, P.; Dsouza, F.; Vogel, E.; Kisters, M.; Medforth, C. J.; Smith, K. M. 1st Reversible Electrogeneration of Triply Oxidized Nickel Porphyrins and Porphycenes Formation of Nickel(Iii) Pi-Dications. *Inorg. Chem.* **1993**, *32*, 4177-4178.
- (16) Walker, F. A.; Huynh, B. H.; Scheidt, W. R.; Osvath, S. R. Models of the Cytochromes-B-Effect of Axial Ligand Plane Orientation on the Electron-Paramagnetic-Res and Mossbauer-Spectra of Low-Spin Ferrihemes. *J. Am. Chem. Soc.* **1986**, *108*, 5288-5297.
- (17) Jia, S. L.; Jentzen, W.; Shang, M.; Song, X. Z.; Ma, J. G.; Scheidt, W. R.; Shelnutt, J. A. Axial Coordination and Conformational Heterogeneity of Nickel(II) Tetraphenylporphyrin Complexes with Nitrogenous Bases. *Inorg. Chem.* **1998**, *37*, 4402-4412.
- (18) Shelnutt, J. A.; Song, X. Z.; Ma, J. G.; Jia, S. L.; Jentzen, W.; Medforth, C. J. Nonplanar Porphyrins and Their Significance in Proteins. *Chem. Soc. Rev.* **1998**, *27*, 31-41.
- (19) Shelnutt, J. A.; Medforth, C. J.; Berber, M. D.; Barkigia, K. M.; Smith, K. M. Relationships between Structural Parameters and Raman Frequencies for Some Planar and Nonplanar Nickel(Ii) Porphyrins. *J. Am. Chem. Soc.* **1991**, *113*, 4077-4087.
- (20) Jentzen, W.; Simpson, M. C.; Hobbs, J. D.; Song, X.; Ema, T.; Nelson, N. Y.; Medforth, C. J.; Smith, K. M.; Veyrat, M.; Mazzanti, M. et al. Ruffling in a Series of Nickel(II) meso-

- Tetrasubstituted Porphyrins as a Model for the Conserved Ruffling of the Heme of Cytochromes c. J. Am. Chem. Soc. **1995**, 117, 11085-11097.
- (21) Gouterman, M. Study of the Effects of Substitution on the Absorption Spectra of Porphin. *J. Chem. Phys.* **1959**, *30*, 1139-1161.
- (22) Rodriguez, J.; Holten, D. Ultrafast Photodissociation of a Metalloporphyrin in the Condensed Phase. *J. Chem. Phys.* **1990**, *92*, 5944-5950.
- (23) Mizutani, Y.; Uesugi, Y.; Kitagawa, T. Intramolecular Vibrational Energy Redistribution and Intermolecular Energy Transfer in the (d,d) Excited State of Nickel Octaethylporphyrin. *J. Chem. Phys.* **1999**, *111*, 8950-8962.
- (24) Chen, L. X.; Zhang, X.; Wasinger, E. C.; Attenkofer, K.; Jennings, G.; Muresan, A. Z.; Lindsey, J. S. Tracking Electrons and Atoms in a Photoexcited Metalloporphyrin by X-ray Transient Absorption Spectroscopy. *J. Am. Chem. Soc.* **2007**, *129*, 9616-9618.
- (25) Campbell, L.; Tanaka, S.; Mukamel, S. Ligand Effects on the X-ray Absorption of a Nickel Porphyrin Complex: a Simulation Study. *Chem. Phys.* **2004**, *299*, 225-231.
- (26) Huang, Q.; Medforth, C. J.; Schweitzer-Stenner, R. Nonplanar Heme Deformations and Excited State Displacements in Nickel Porphyrins Detected by Raman Spectroscopy at Soret Excitation. *J. Phys. Chem. A* **2005**, *109*, 10493-10502.
- (27) Drain, C. M.; Gentemann, S.; Roberts, J. A.; Nelson, N. Y.; Medforth, C. J.; Jia, S.; Simpson, M. C.; Smith, K. M.; Fajer, J.; Shelnutt, J. A. et al. Picosecond to Microsecond Photodynamics of a Nonplanar Nickel Porphyrin: Solvent Dielectric and Temperature Effects. *J. Am. Chem. Soc.* **1998**, *120*, 3781-3791.
- (28) Shelby, M. L.; Lestrange, P. J.; Jackson, N. E.; Haldrup, K.; Mara, M. W.; Stickrath, A. B.; Zhu, D.; Lemke, H. T.; Chollet, M.; Hoffman, B. M. et al. Ultrafast Excited State Relaxation of a Metalloporphyrin Revealed by Femtosecond X-ray Absorption Spectroscopy. *J. Am. Chem. Soc.* **2016**, *138*, 8752-8764.
- (29) Shelby, M. L.; Mara, M. W.; Chen, L. X. New Insight into Metalloporphyrin Excited State Structures and Axial Ligand Binding from X-ray Transient Absorption Spectroscopic Studies. *Coord. Chem. Rev.* **2014**, *277-278*, 291-299.
- (30) Chen, L. X.; Shelby, M. L.; Lestrange, P. J.; Jackson, N. E.; Haldrup, K.; Mara, M. W.; Stickrath, A. B.; Zhu, D.; Lemke, H.; Chollet, M. et al. Imaging Ultrafast Excited State Pathways in Transition Metal Complexes by X-ray Transient Absorption and Scattering using X-ray Free Electron Laser Source. *Faraday Discuss.* **2016**, *194*, 639-658.
- (31) Senge, M. O.; Feng, X. D. Regioselective Reaction of 5,15-disubstituted Porphyrins with Organolithium Reagents Synthetic Access to 5,10,15-trisubstituted Porphyrins and Directly Meso-meso-linked Bisporphyrins. *Perkin Trans.* **2000**, *21*, 3615-3621.
- (32) Senge, M. O. A Conformational Study of 5,10,15,20-tetraalkyl-22H(+),24H(+) Porphyrindiium Salts (Dication Salts). *Z. Naturforsch. B Chem. Sci.* **2000**, *55*, 336-344.
- (33) Liu, Q.; Tang, M.; Zeng, W.; Zhang, X.; Wang, J.; Zhou, Z. Optimal Size Matching and Minimal Distortion Energy: Implications for Natural Selection by the Macrocycle of the Iron Species in Heme. *Eur. J. Inorg. Chem.* **2016**, *2016*, 5222-5229.
- (34) Kau, L. S.; Spira-Solomon, D. J.; Penner-Hahn, J. E.; Hodgson, K. O.; Solomon, E. I. X-ray Absorption Edge Determination of the Oxidation State and Coordination Number of Copper. Application to the Type 3 Site in Rhus Vernicifera Laccase and its Reaction with Oxygen. *J. Am. Chem. Soc.* **1987**, *109*, 6433-6442.
- (35) Ravel, B.; Newville, M. Athena, Artemis, Hephaestus: Data Analysis for X-ray Absorption Spectroscopy using IFEFFIT, *J. Synchrotron Rad.* **2005**, *12*, 537-541.

- (36) Longuet-Higgins, H. C.; Rector, C. W.; Platt, J. R. Molecular Orbital Calculations on Porphine and Tetrahydroporphine. *J. Chem. Phys.* **1950**, *18*, 1174-1181.
- (37) Retsek, J. L.; Drain, C. M.; Kirmaier, C.; Nurco, D. J.; Medforth, C. J.; Smith, K. M.; Sazanovich, I. V.; Chirvony, V. S.; Fajer, J.; Holten, D. Photoinduced Axial Ligation and Deligation Dynamics of Nonplanar Nickel Dodecaarylporphyrins. *J. Am. Chem. Soc.* **2003**, *125*, 9787-9800.
- (38) Kim, D.; Kirmaier, C.; Holten, D. Nickel Porphyrin Photophysics and Photochemistry. A Picosecond Investigation of Ligand Binding and Release in the Excited State. *Chem. Phys.* **1983**, *75*, 305-322.
- (39) Zhang, X.; Wasinger, E. C.; Muresan, A. Z.; Attenkofer, K.; Jennings, G.; Lindsey, J. S.; Chen, L. X. Ultrafast Stimulated Emission and Structural Dynamics in Nickel Porphyrins. *J. Phys. Chem. A* **2007**, *111*, 11736-11742.
- (40) Mizutani, Y.; Teizo, K. Mode Dependence of Vibrational Energy Redistribution in Nickel Tetraphenylporphyrin Probed by Picosecond Time-Resolved Resonance Raman Spectroscopy: Slow IVR to Phenyl Peripherals. *Bull. Chem. Soc. Jpn* **2002**, *75*, 965-971.

